Fatimah et al. Sustainable Environment Research (2019) 29:40
https://doi.org/10.1186/s42834-019-0034-3

Sustainable Environment Research

RESEARCH Open Access

Functionalization of hydroxyapatite derived from cockle (*Anadara granosa*) shells into hydroxyapatite–nano TiO_2 for photocatalytic degradation of methyl violet

Is Fatimah[1*], Della Fahrani[1], Tia Harmawantika[1], Imam Sahroni[1], Azlan Kamari[2], Cecep Sa'bana Rahmatillah[1] and Rico Nurillahi[1]

Abstract

Photocatalyst of hydroxyapatite–nano TiO_2 (HAp-*n*TiO_2) was prepared from phosphatation of calcined cockle (*Anadara granosa*) shells followed by dispersion of nano TiO_2 powder into HAp precipitate and calcination at 400 °C for 2 h. The prepared material was characterized using X-ray diffraction, scanning electron microscope–energy dispersive X-ray spectrophotometry, gas sorption analysis, and UV-Vis diffuse reflectance spectrophotometry. The photocatalytic activity of the material was evaluated for methyl violet degradation over photocatalysis and photooxidation mechanism. The results showed that the homogeneous dispersion of TiO_2 in the HAp-*n*TiO_2 composite was achieved, as seen in the X-ray diffraction analysis, diffuse reflectance UV-Vis, and gas sorption analyses. The physicochemical and photocatalytic character of the composite exhibited the positive role of HAp as TiO_2 support in enhancing the photocatalytic activity with a higher turnover number and reusability property than that of pure TiO_2. It was also noted that the HAp-*n*TiO_2 composite demonstrated rapid methyl violet degradation over photooxidation rather than by photocatalytic mechanism.

Keywords: Photocatalyst, Adsorption, Degradation, Methyl violet

Introduction

Photocatalysis is a developed technology with many wastewater treatment applications, one of which is the treatment of dye-containing wastewater from industries like textiles, painting, printing, and other related industries [1]. It has been reported that approximately 10–15 wt% of the dyes used in textile industries are discharged as wastewater [2, 3]. With the presence of mainly stable organic compounds, a powerful photocatalyst is required for the photooxidation process in treating dye-containing wastewater. Among metal oxide photocatalysts, such as ZnO, ZrO_2, and Fe_2O_3, TiO_2 is the most popular photocatalyst material given its low cost, non-toxicity, and effective band gap energy that sufficiently supports an economic photocatalysis process [4]. Along with the exploration of low-cost processes for photocatalysis, some modifications have been attempted to enhance the photocatalytic activity of TiO_2 [5–7]. The preparation of composites containing TiO_2 has been reported as offering several advantages related to material stability [8]. The use and conversion of waste materials into functional materials has also received intensive attention. In line with this exploration of sustainable materials, the conversion of calcium-containing animal waste into valuable materials has been reported. Significant research has reported the utilization of CaO derived from snail shells, egg shells, and fish bones for the preparation of calcium-based materials, such as hydroxyapatite (HAp), perovskite, and other composites, together with other metal oxides or minerals [9–12]. The use of animal shells from scallops, snails, and cockles, as well as fish bones, has been reported for these purposes [13–15]. The simple conversion of these waste materials into

* Correspondence: isfatimah@uii.ac.id
[1]Chemistry Department, Universitas Islam Indonesia, Yogyakarta 55584, Indonesia
Full list of author information is available at the end of the article

CaO (sometimes called biogenic CaO), which requires calcination at approximately 600–1200 °C, is the challenge for the preparation of functional material.

HAp [$Ca_{10}(PO_4)_6(OH)_2$] is a material that can be prepared from biogenic CaO through sol-gel synthesis and precipitation, among other techniques. Some examples of HAp preparation are the conversion of oyster shells and rice field snail shells into HAp using precipitation [9, 16], a sol-gel method of converting snail shells [17], and a microwave-assisted preparation [18] of snail shells. Among its potential uses, HAp has been reported as effective in enhancing TiO_2 photocatalytic activity, and HAp prepared from waste mussel shells has been reported to be active in catalyzing dye oxidation. The combination of HAp and TiO_2 was reported to produce developed microstructures, the phases of which are useful for densification and the mechanical properties of the composite [19]. Several investigations have remarked upon the improved performance of photocatalysis profiles by the combination and/or dispersion of TiO_2 with HAp. The enhanced performance was influenced by the coating effect of HAp and the supporting adsorption capability involved in the photocatalysis mechanism [20–23]. Based on our previous research into the preparation of HAp from biogenic CaO and other investigations of the photocatalytic activity of nano TiO_2 [4, 18], this research aims to investigate the preparation of HAp–nano TiO_2 composite for dye photodegradation applications. Among CaO sources, *Anadara granosa* shell was interesting to be explored since it has been cultivated for its meat that highly consumed, so it produces shell as waste in large amount. The research focused on physicochemical property evolution from the biogenic CaO into the HAp–nano TiO_2 (HAp-$n$$TiO_2$) composite and the evaluation of the photocatalytic activity of the material.

Materials and methods

Cockle shells were obtained from beaches in Yogyakarta Province, Indonesia; methyl violet (MV), aquadest, ammonium phosphate [$(NH)_4HPO_4$], Whatman 41 filter paper, potassium hydrogen phthalate, potassium bichromate, hydrogen peroxide (H_2O_2), ethanol, $n$$TiO_2$, and ammonium hydroxide (NH_4OH) were purchased from Merck-Millipore (Germany).

Preparation of HAp and HAp-nTiO$_2$

Cockle shells were crushed using hammer followed by grounding. The first step was converting cockle shells into CaO by calcination at 1000 °C for 3 h, and the powder of biogenic CaO was obtained. The obtained CaO powder of 15 g was diluted into 200 mL of distilled water, and then diammonium hydrogen phosphate solution was slowly added under stirring. The molar ratio of Ca/P was set as 1.67. The mixture was stirred overnight before being filtered off and calcined at 400 °C for 2 h. The powder obtained from these steps was the prepared HAp.

Preparation of HAp-$n$$TiO_2$ began with the preparation of HAp, described above. After the mixture of CaO and diammonium hydrogen phosphate solution was precipitated, nano TiO_2 was added into the precipitate at the theoretic Ti content set up at 5 wt%. The mixture was then stirred overnight, filtered off, and dried. The dry

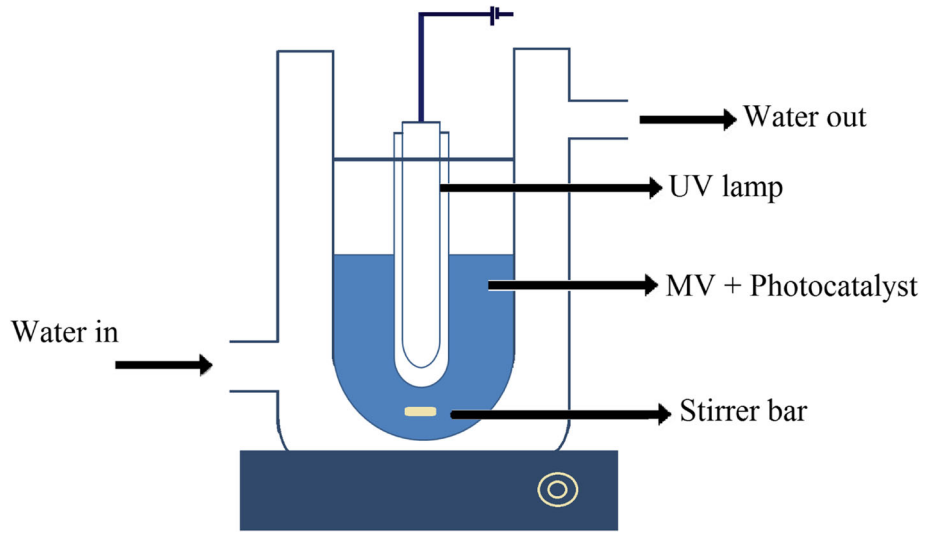

Fig. 1 Schematic representation of photocatalytic reactor

powder was calcined at 400 °C for 2 h, and the powder sample was designated as HAp- nTiO$_2$.

Material characterization

Analysis of the materials was conducted using X-ray diffraction (XRD), scanning electron microscope–energy dispersive X-ray (SEM-EDX) spectrophotometry analysis, UV-Vis diffuse reflectance spectrophotometry (UV-DRS), gas sorption analysis, and Fourier transform infrared (FTIR) spectrometry. XRD patterns were recorded using a Rigaku Miniflex with Ni-filtered Cu-Kα as a radiation source. The reflections obtained were recorded in the range of 2θ of 10–70° and a step size of 0.2° min^{-1}. Gas sorption analysis was performed using the Quantachrome NOVA 1200e instrument. The samples were degassed at 90 °C for 6 h prior to liquid N_2 adsorption at 77 K. SEM (JSM-5410, JEOL, Japan) was employed for surface image and elemental analyses, UV-DRS (JASCO, Japan) was used for diffuse reflectance spectra, and an FTIR spectrometer (Perkin Elmer, USA) was used for the functional group analysis. The spectra obtained were in the range of 4000–400 cm^{-1}.

Photocatalytic activity test of HAP-nTiO$_2$ composite

The photocatalytic activity of HAp-nTiO$_2$ was evaluated in MV photocatalysis and photooxidation by using a photocatalytic reactor equipped with a UVB Lamp (20 W, Philips, USA) placed in the inner part of the batch reactor, as presented in Fig. 1.

For each experiment, the mixture of 1 L of MV solution and 0.25 g photocatalyst was placed in the reactor and was exposed by UV light at the pH of 7. Two varied treatments were prepared: photocatalysis and photooxidation; the difference is the absence or presence of H_2O_2 as an oxidant, respectively. The degradation efficiency was calculated based on the change of MV before and after treatment using the following Eq. (1):

$$Degradation\ efficiency = \frac{C_o - C_t}{C_o} x100\% \quad (1)$$

C_o and C_t are MV concentrations at initial and time of t, respectively. Those concentrations were spectrophotometric determined using UV-Vis spectrophotometric analysis was performed with the wavelength of 583 nm. Spectrophotometer HITACHI U-2010 was utilized. Identification of MV degradation was performed by high performance liquid chromatography (HPLC) analysis. For HPLC, Waters Alliance e2695 (Milford, MA, USA) was employed. Kinetex C18 100A column was used for analysis using 0.1% formic acid in acetonitrile and water as mobile phase (1:1), and UV detector at 214 nm.

Results and discussion

Physicochemical character of materials

Figure 2 shows the XRD patterns for biogenic CaO derived from calcination of cockle shells, HAp, and HAp-nTiO$_2$ samples. The pattern of CaO shows a major phase of calcite, confirmed by reference to JCPDS card no. 5–586, with some peaks associated with the presence of aragonite in small intensities as an indication of the incomplete conversion of $CaCO_3$ into CaO. The pattern is similar to biogenic CaO derived from other animal shells, such as mussels, cockles, and scallops [19, 24].

From the XRD pattern of the HAp sample, it can be concluded that HAp was successfully prepared as confirmed by the fitness with the pattern of JCPDS no. 09–0432 (pure HAp). However, small intensity reflections

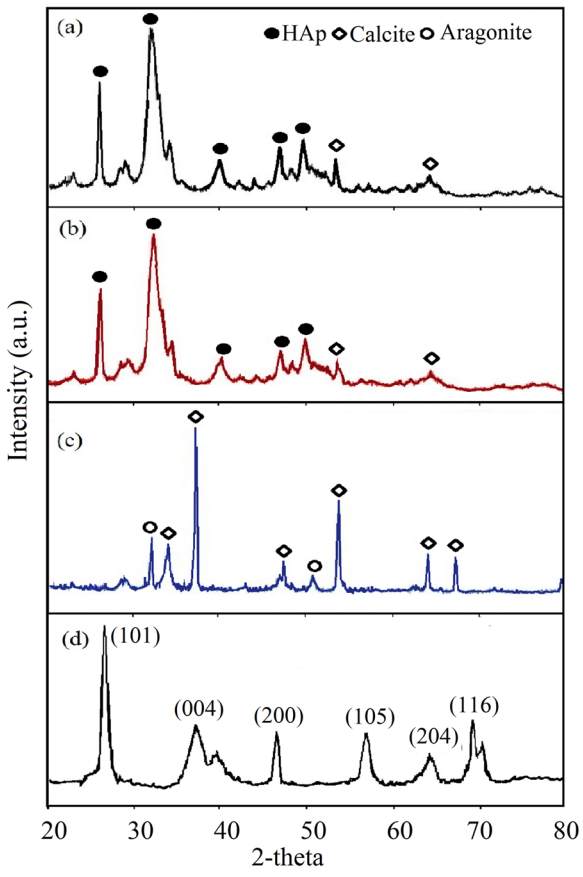

Fig. 2 XRD pattern of (**a**) HAp-nTiO$_2$, (**b**) HAp, and (**c**) CaO derived from *Cockle* shell (**d**) nano-TiO$_2$

indicated the presence of calcite at 52.9° and 64°, implying incomplete conversion of Ca to HAp. This is similar to a pattern that was reported in the preparation of HAp from snail (*Achatina achatina*) shells [25]. Referring to the reflection of nano TiO_2, it can be seen that there was no significant difference detected in the HAp-*n*TiO_2 reflection with respect to the HAp. There is no new reflection associated with the presence of TiO_2 in any phase, which was likely related to the homogeneous dispersion of nano TiO_2 in the porous structure of HAp [26]. The absence of an *n*TiO_2 reflection in the composite is an indication of the absence of TiO_2 aggregation in the composite formation, meaning that TiO_2 was homogeneously dispersed in the composite form. The data can be confirmed by reference to previous similar work on TiO_2 dispersion onto HAp, which reported the relatively low intensity peak of TiO_2 along with decreasing TiO_2 content in the composition [20, 27].

The presence of Ti was identified by EDX analysis. The surface profile depicted by SEM analysis (Fig. 3) exhibits

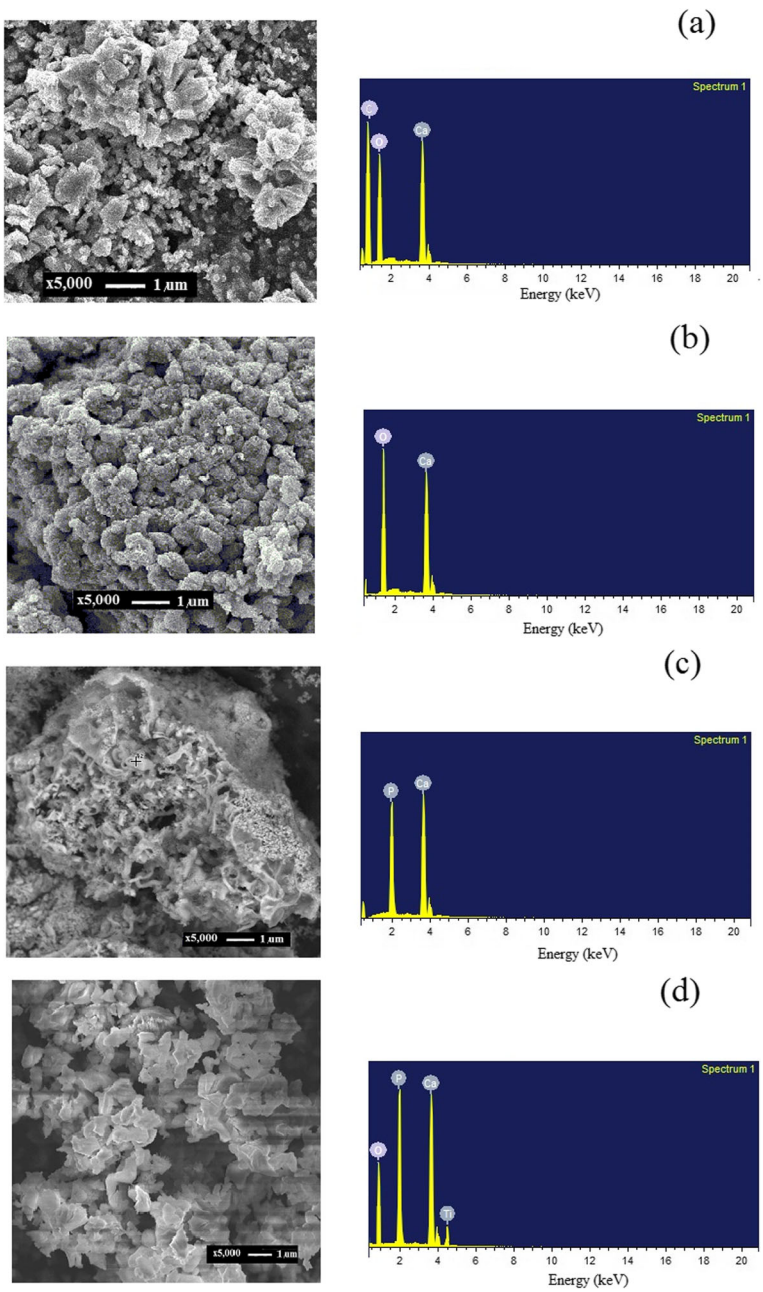

Fig. 3 SEM profile and EDX spectra of (**a**) *Cockle* shell, (**b**) CaO, (**c**) HAp, and (**d**) HAp-*n*TiO_2

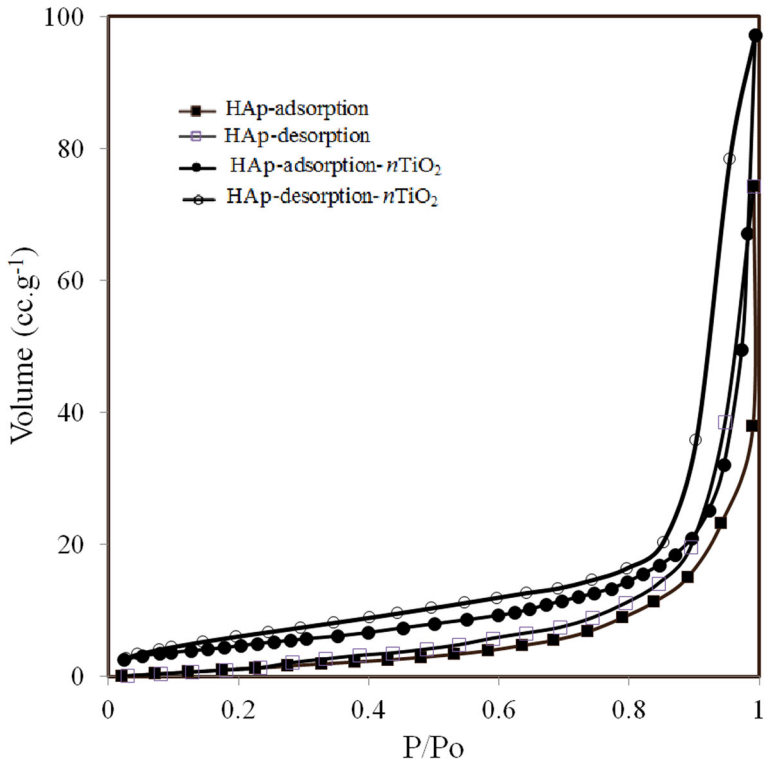

Fig. 4 Adsorption-desorption profile of HAp and HAp-nTiO$_2$

the increased open surface found in HAp-nTiO$_2$ compared to HAp, CaO, and raw cockle shells. The change in chemical composition of the material was also seen, changing from the Ca, C, and O, the major components of cockle shells, to Ca and O for derived CaO, and to Ca and P for HAp. The ratio of Ca/P in HAp is 1.68, slightly higher than the stoichiometric ratio of 1.67, which was likely caused by the excess Ca content of CaO converted by cockle shell calcination. Ti content in HAp-nTiO$_2$ was found at 4.43 at%, or equal to about 7.4 wt% of TiO$_2$, which is also slightly lower than the targeted content of 5 at%. The TiO$_2$ attachment in the composite showed the effect on the surface profile, identifiable via the gas sorption analysis with the adsorption-desorption isotherm depicted in Fig. 4; the calculated parameters of specific surface area, pore volume, and pore radius, along with the EDX analysis results, are presented in Table 1. The composite has the same pattern of isotherm as HAp, but with

Table 1 Surface parameters and elemental analysis result of materials

Parameter	CaO	HAp	HAp-nTiO$_2$	TiO$_2$
Specific surface area ($m^2\ g^{-1}$)	21 ± 0.02	56 ± 0.03	62 ± 0.05	78 ± 0.05
Pore volume ($cc\ g^{-1}$)	0.10 ± 0.02	0.46 ± 0.01	0.51 ± 0.02	0.55 ± 0.02
Pore radius (Å)	174 ± 0.12	165 ± 0.11	163 ± 0.21	154 ± 0.17
Band gap energy (eV)	n.d*	n.d	3.21	3.21
Ca (wt%)	23.5 ± 0.03	20.12 ± 0.02	34.70 ± 0.02	–
O (wt%)	73.8 ± 0.06	67.80 ± 0.05	44.24 ± 0.09	60.47 ± 0.05
P (wt%)	n.d	11.99	20.34 ± 0.01	–
Ti (wt.)	n.d	n.d	4.43 ± 0.06	38.98 ± 0.05
TiO$_2$ (wt%)			7.40 ± 0.03	99.99 ± 0.01

n.d Not detected

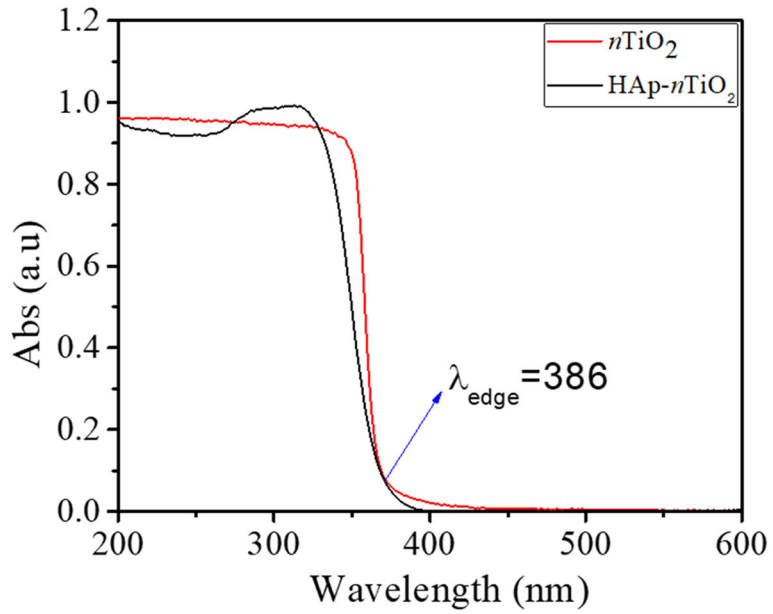

Fig. 5 DRUV- Visible spectra of HAp-nTiO$_2$ and TiO$_2$

higher adsorbed volume at a range of P/Po. From the isotherm, it was found that the specific surface area and pore radius of HAp-nTiO$_2$ were higher than those of HAp.

The attached TiO$_2$ in the HAp-nTiO$_2$ contributes to the band gap energy as shown by UV-DRS spectra in Fig. 5. HAp-nTiO$_2$ shows the band gap energy of 3.21 eV, which is the same value as the band gap energy of nTiO$_2$. The slight shift of the absorption in the range of 300–400 nm revealed the interaction between HAp and TiO$_2$ [20]. The same value is in line with the XRD data, which indicates that nTiO$_2$ is homogeneously dispersed in the HAp matrix.

Kinetics of photodegradation

Figure 6 shows the treatment-varying plot of the percentage of degradation to the photodegradation process of MV using HAp-nTiO$_2$, HAp, and TiO$_2$. Three treatments—adsorption, photocatalysis, and photooxidation—were examined to evaluate the role of the photocatalyst. Adsorption is the treatment of photocatalyst addition without H_2O_2 under dark conditions, while photocatalysis and photooxidation are treatments under UV exposure, distinguished by the addition of H_2O_2 as an oxidant for the photooxidation treatment. From the curve, it can be seen that, in general, the photocatalytic and photooxidation treatments showed higher photodegradation efficiency with respect to adsorption. Significant degradation was demonstrated in photooxidation and photocatalysis using HAp-nTiO$_2$, TiO$_2$, and HAp.

A comparison of kinetics data revealed that TiO$_2$ is the superior photocatalyst, and affected by the H_2O_2 concentration. The total photoactive surface of TiO$_2$ plays an intensive role in the MV degradation.

In contrast, both photocatalysis and photooxidation using HAp showed lower efficiency compared with the use of HAp-nTiO$_2$ andTiO$_2$ during the monitored time of treatment. The absence of photoactive material is the main point of significance for the data, which is in line with previously reported research that revealed the band gap energy of HAp is 4.85 eV, exceeding the exciting limit of the used UV lamp [28]. The MV degradation is likely caused by the photolysis effect forced by surface activation in the presence of UV exposure [29, 30]. The kinetics data (Table 2) confirmed the effect of the addition of H_2O_2 to the increasing MV degradation by using all photocatalysts.

The accelerating rate of degradation is revealed by the increasing initial rate and kinetics constant of reactions. All reactions obey pseudo–first order kinetics. From the data, kinetics constants of photooxidation using all photocatalysts are shown to be higher compared to the values from photocatalysis, meaning the faster reaction is obtained by photooxidation. In general, for all photocatalysts, photooxidation occurred more quickly than photocatalysis. This is in line with the theoretical approach and some previous research on dye degradation enhanced by the presence of oxidant. The presence of H_2O_2 enhances the oxidation mechanism due to its cleavage to form •OH, which

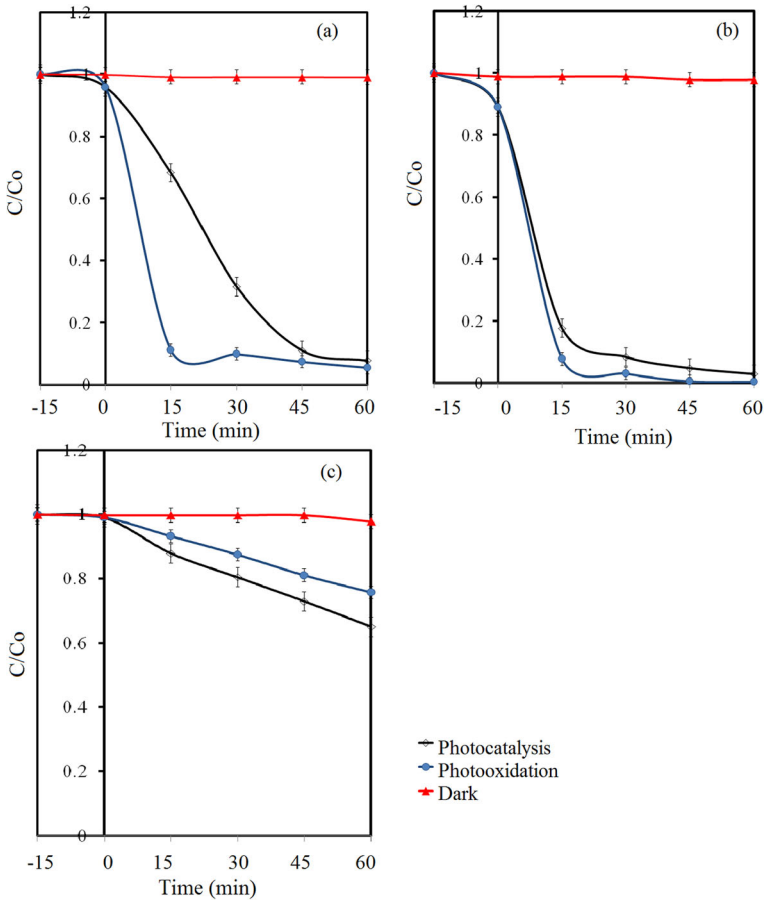

Fig. 6 Kinetics of MV degradation by using (**a**) HAp-*n*TiO_2, (**b**) TiO_2, and (**c**) HAp [Initial MV concentration = 25 mg L^{-1}, $H_2O_2 = 10^{-4}$ M, catalyst dosage = 0.25 g L^{-1}]

poses as a strong oxidant referring to the following mechanisms (2–6): [5].

$$TiO_2 + h\nu \rightarrow e^-_{cb} + h^+_{vb} \quad (2)$$

$$e^- + O_{2(ads)} \rightarrow O_{2(ads)}\bullet \quad (3)$$

$$e^- + H^+_{ads} \rightarrow H\bullet_{ads} \quad (4)$$

$$O_{2(ads)}\bullet + H^+_{ads} \rightarrow HOO\bullet \quad (5)$$

$$H_2O_2 + O_{2(ads)}\bullet \rightarrow \bullet OH + {}^-OH + O_2 \quad (6)$$

The interaction between photoactive semiconductor (TiO_2) and photon (UV light) generates hydroxyl radicals at the surface of the photocatalyst and the conduction band (e^-), which potentially negatively reduces molecular oxygen. The generation of hydroxyl radicals and oxidant agents will be rapidly enhanced in the presence of H_2O_2 [1, 2].

The increasing rate was confirmed by the UV-Vis spectra of the treated solution (Fig. 7). The molecular structure degradation of MV is revealed not only by the decreasing absorbance of the maximum

Table 2 Kinetics equation and parameters of MV photocatalysis and photooxidation using varied photocatalysts

Photocatalyst	Photocatalysis			Photooxidation		
	Initial rate (mg L^{-1} min^{-1})	k (min^{-1})	R^2	Initial rate (mg L^{-1} min^{-1})	k (min^{-1})	Kinetics equation (R^2)
HAp	1.9	4.5×10^{-3}	0.9991	2.8	6.9×10^{-3}	0.9988
HAp-*n*TiO_2	7.3	4.1×10^{-2}	0.9917	7.7	4.6×10^{-2}	0.9778
TiO_2	7.7	5.5×10^{-2}	0.9688	7.9	9.5×10^{-2}	0.9770

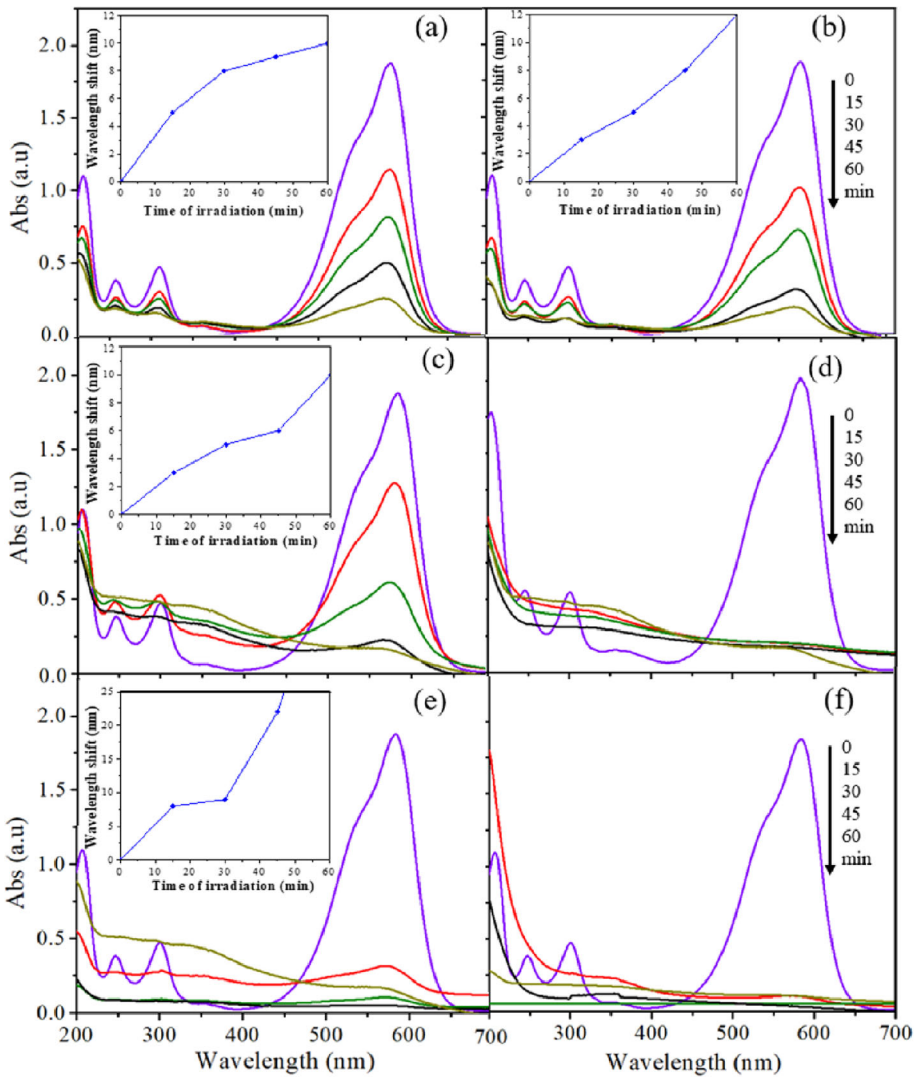

Fig. 7 UV-Visible spectra of treated solution by (**a**) photocatalysis using HAp, (**b**) photooxidation using HAp, (**c**) photocatalysis using HAp-*n*TiO_2, (**d**) photooxidation using HAp-*n*TiO_2, (**e**) photocatalysis using TiO_2, and (**f**) photooxidation using TiO_2 [Initial MV concentration = 25 mg L^{-1}, $H_2O_2 = 10^{-4}$ M, catalyst dosage = 0.25 g L^{-1}]

wavelength in the visible region spectrum (593 nm), but also by the red shift of the spectrum, which is higher with increasing time of treatment, indicating de-methylation of the MV structure [31]. It was also noted that the degradation via de-methylation by photooxidation was the fastest using TiO_2 as the photocatalyst, while the slowest occurred from photocatalysis using HAp. Degradation efficiency of almost 100% was seen in photooxidation under TiO_2 after 45 min of treatment.

The extent of the degradation was proven from HPLC chromatograms depicted in Fig. 8. The initial solution showed a single peak at the retention time of 6.0 min as an indication of MV. The peak area was reduced along time of treatment, together with the presence of other peaks at 4.9 and 6.4 min, indicating the oxidation intermediate compounds. These changes are in line with the reduction of COD values from 22 mg L^{-1} at initial to 4.2 mg L^{-1} by photooxidation and to approximately 8.2 mg L^{-1} by photocatalysis after 60 min of treatment.

In terms of catalyst efficiency, the turnover number (TON) is an important parameter. The TON is the quantity of reactant molecules that are converted into products in the presence of a certain weight, specific surface area, or specified active species in

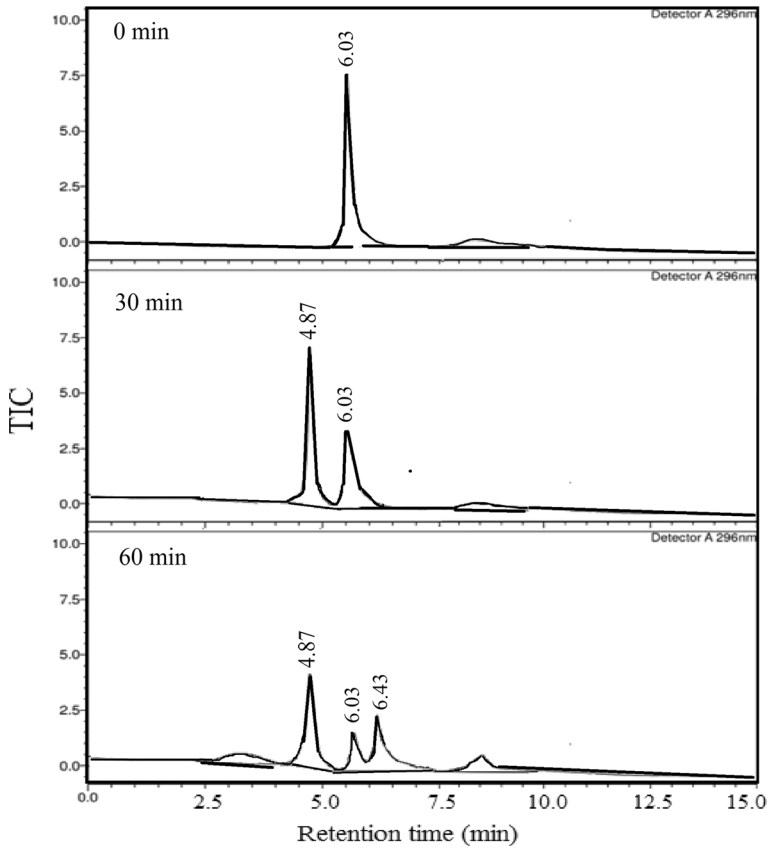

Fig. 8 Chromatogram from HPLC analysis of MV photooxidation treatment [Initial MV concentration = 25 mg L^{-1}, $H_2O_2 = 10^{-4}$ M, catalyst dosage = 0.25 g L^{-1}]

the catalyst [32]. Referring to the elemental analysis results tabulated in Table 3, which show the Ti content of 4.43 at%, meaning that TiO_2 content is 7.4 wt%, the TON of reaction using HAp-TiO_2 was calculated based on 7.4 wt%. TiO_2 with the 100 wt% value used for the pure nano TiO_2. The degradation efficiency and TON obtained from 30 min of photocatalysis and photooxidation treatment using HAp-*n*TiO_2 and TiO_2 are presented in Fig. 9. The degradation efficiency and TON were evaluated at varied catalyst dosages: 0.25, 0.50, and 1.0 g L^{-1}. The TON values of the photocatalysis increased as increasing catalyst dosage within the range of 77–84%, while for the photooxidation, the values are ranging from 81 to 97%. These TON values are comparable with the TON values in MV photodegradation by using $TiSiW_{12}O_{40}/TiO_2$ [33]. Refer to the TiO_2 content of 1.35 wt% and the degradation yield at 30 min by using photocatalyst dosage of 0.15–0.30 g L^{-1}, the TON values are ranging from 77 to 88%. Comparability is also found due to the photocatalytic activity of the same composites of TiO_2/HAp for methyl orange and methylene blue photocatalytic degradation [34, 35]. With the degradation efficiency of 33% at 30 min by TiO_2 content of 8.06 wt% in HAp/TiO_2 composite and the catalyst dosage of 20 mg L^{-1},

Table 3 Langmuir-Hinshelwood parameters of MV photocatalysis and photooxidation

Photocatalyst	Photocatalysis			Photooxidation		
	k_c (mg L^{-1} min^{-1})	K_{LH} (mg^{-1} L)	R^2	k_c (mg L^{-1} min^{-1})	K_{LH} (mg^{-1} L)	R^2
HAp-*n*TiO_2	22	1606	0.9998	32	1027	0.9999
TiO_2	8	256	0.9940	7	162	0.9984

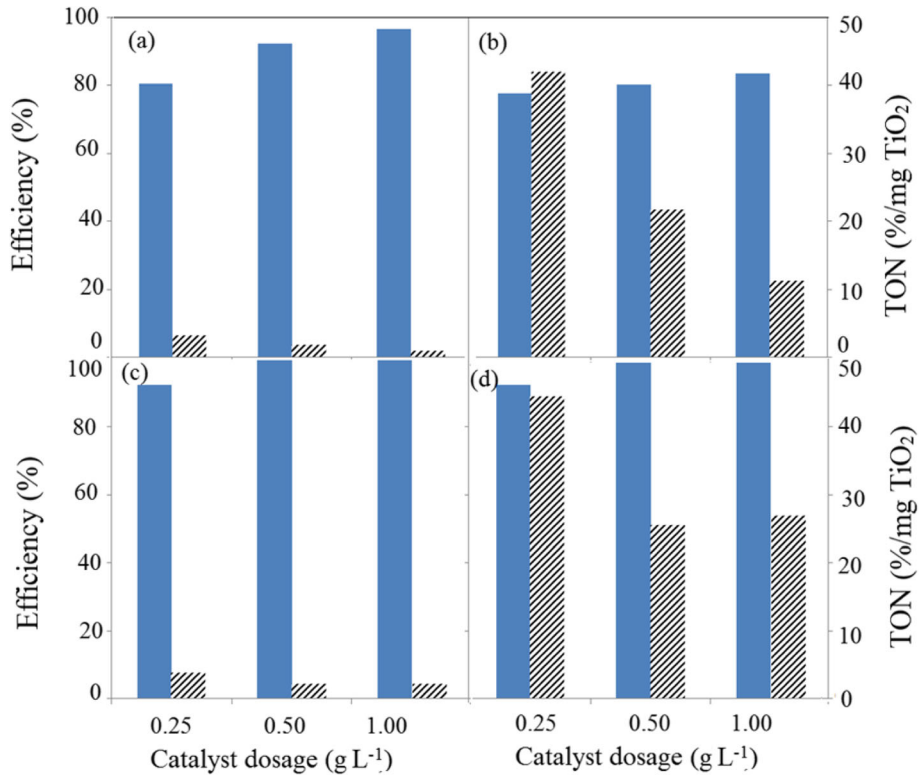

Fig. 9 Degradation efficiency and TON at varied photocatalyst dosage of (**a**) photooxidation using TiO_2, (**b**) photooxidation using HAp-$n$$TiO_2$, (**c**) photocatalysis using TiO_2, and (**d**) photocatalysis using HAp-$n$$TiO_2$ [Initial MV concentration = 25 mg L^{-1}, $H_2O_2 = 10^{-4}$ M, TON values are calculated from 30 min of treatment]

photocatalytic degradation of methyl orange gives the TON value of 82% [34]. Moreover, the photocatalytic degradation of methylene blue by TiO_2/HAp with TiO_2 content of 40 wt% gives the TON of 113% [35], and from other similar research with the TiO_2 content of 5.01, 10.02, and 18.37 wt%, the TON are ranging from 60 to 80% [30].

From the above discussion, the use of HAp-$n$$TiO_2$ instead of TiO_2 should be made due to the higher TON as the indication of more efficient photocatalytic material. Moreover, the use of Cockle shells in this research is an advantage related to the sustainability of raw material for HAp synthesis.

Effects of the initial MV concentration on the photocatalysis and photooxidation rates using HAp-$n$$TiO_2$ as a photocatalyst can be seen by the kinetic curve in Fig. 10a–b. Both treatments obey pseudo–first order kinetics in all initial concentration ranges (Fig. 10b). Given numerous investigations on dye photodegradation, the dependence of the reaction rates on the concentration of the dye can be well described by the Langmuir–Hinshelwood (L–H) kinetic model [30, 33, 34] as:

$$\frac{1}{r_o} = \frac{1}{k_c K_{LH}[C_0]} + \frac{1}{k_c} \tag{7}$$

Here, r_o is the initial rate of degradation, C_0 is the initial concentration of MV (mg L^{-1}), K_{LH} is the L-H adsorption constant (mg^{-1} L), and k_c is the rate constant of surface reaction (mg L^{-1} min^{-1}). The values of k_c and K_{LH} describe the limiting rate constants of reaction at maximum coverage of the photocatalyst surface under the given experimental conditions and the equilibrium constant for adsorption of MV onto the photocatalyst, respectively. The L–H plots are presented in Fig. 10c.

The plot of $1/r_0$ versus $1/C_0$ shows a linear variation for all treatments using HAp-$n$$TiO_2$ and TiO_2 photocatalysts, confirming the fitness of the L-H relationship for the initial rates of degradation. The higher the initial concentration of MV, the faster the degradation, which fits into the general theory of reaction rates. The values of k_c and K_{LH} calculated from the equation are listed in Table 3. The photooxidation process gives higher k_c values, which describe the higher apparent kinetics constants. The data are consistent with the

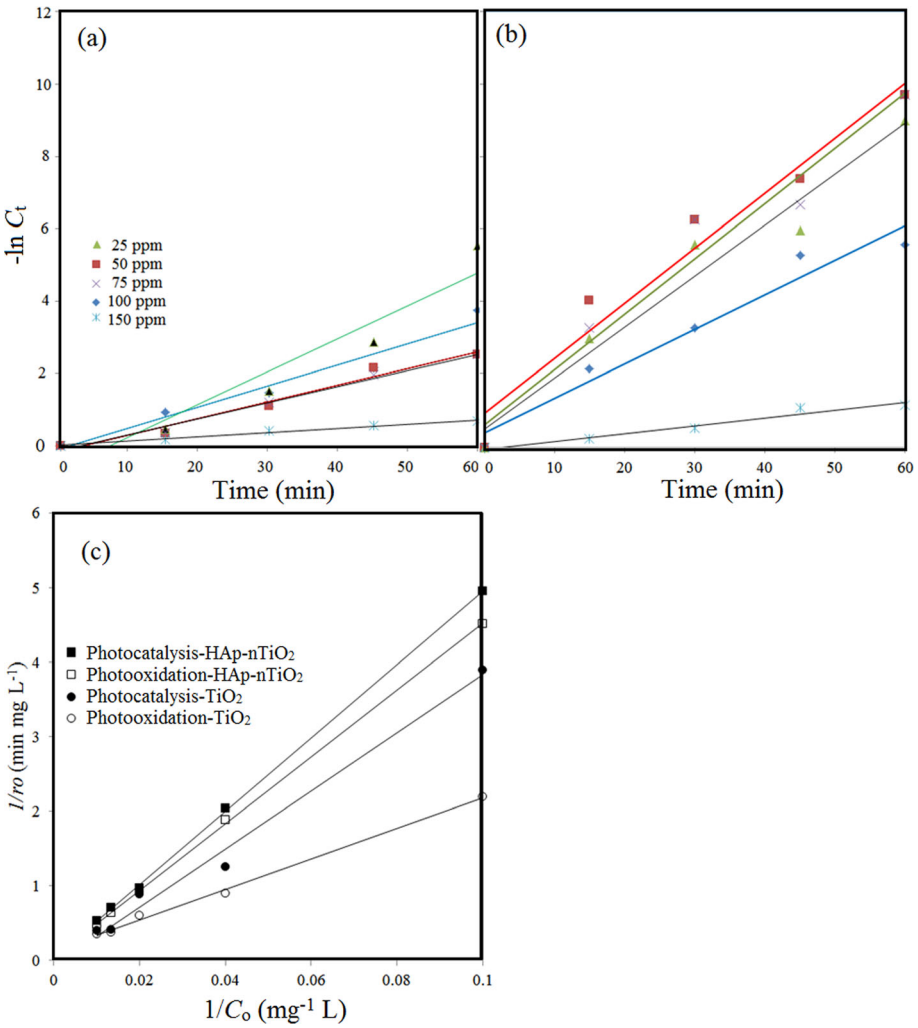

Fig. 10 a Pseudo-first order kinetics plot of photocatalysis using HAp-nTiO$_2$, (**b**) Pseudo-first order kinetics plot of photooxidation using HAp-nTiO$_2$, and (**c**) Langmuir-Hinshelwood plot photocatalysis and photooxidation treatments using HAp-nTiO$_2$ and TiO$_2$

possible oxidation mechanism being accelerated in the presence of H_2O_2 as an oxidant.

Reusability test of the HAp-nTiO$_2$ photocatalyst

HAp-nTiO$_2$ reusability was observed by the kinetics profile and degradation efficiency as presented in Fig. 11. From these patterns, it was concluded that there was no significant change in kinetics profile between the first and the third uses. In contrast, significant reduction of activity appeared in TiO$_2$ utilization at the second and third uses. The reduction in degradation efficiency was most likely due to the loss of the photocatalyst surface active sites after the first use. Similar patterns have also been reported by the use of nanoparticles as photocatalysts [36–38]. From this comparison, it can also be confirmed that HAp plays a role in stabilizing TiO$_2$ in the photocatalysis mechanism.

Conclusions

HAp-nTiO$_2$ composite was successfully prepared using HAp powders derived from cockle (*A. granosa*) shells. The results indicated that HAp was completely formed, as shown by the XRD pattern, and, furthermore, that the nTiO$_2$ was homogeneously dispersed in the composite. The dispersion of nTiO$_2$ in the composite resulted in increasing specific surface area, pore volume, and in the band gap energy having the same value as nTiO$_2$. The composite exhibited photocatalytic activity for photocatalysis and photooxidation of MV. The photocatalytic processes under HAp-nTiO$_2$ and nTiO$_2$ fit well with the L-H model. The use of HAp-nTiO$_2$ gave a higher TON for the processes, which was attributed to the more effective photocatalysis compared to the use of pure nTiO$_2$ for the same reactions.

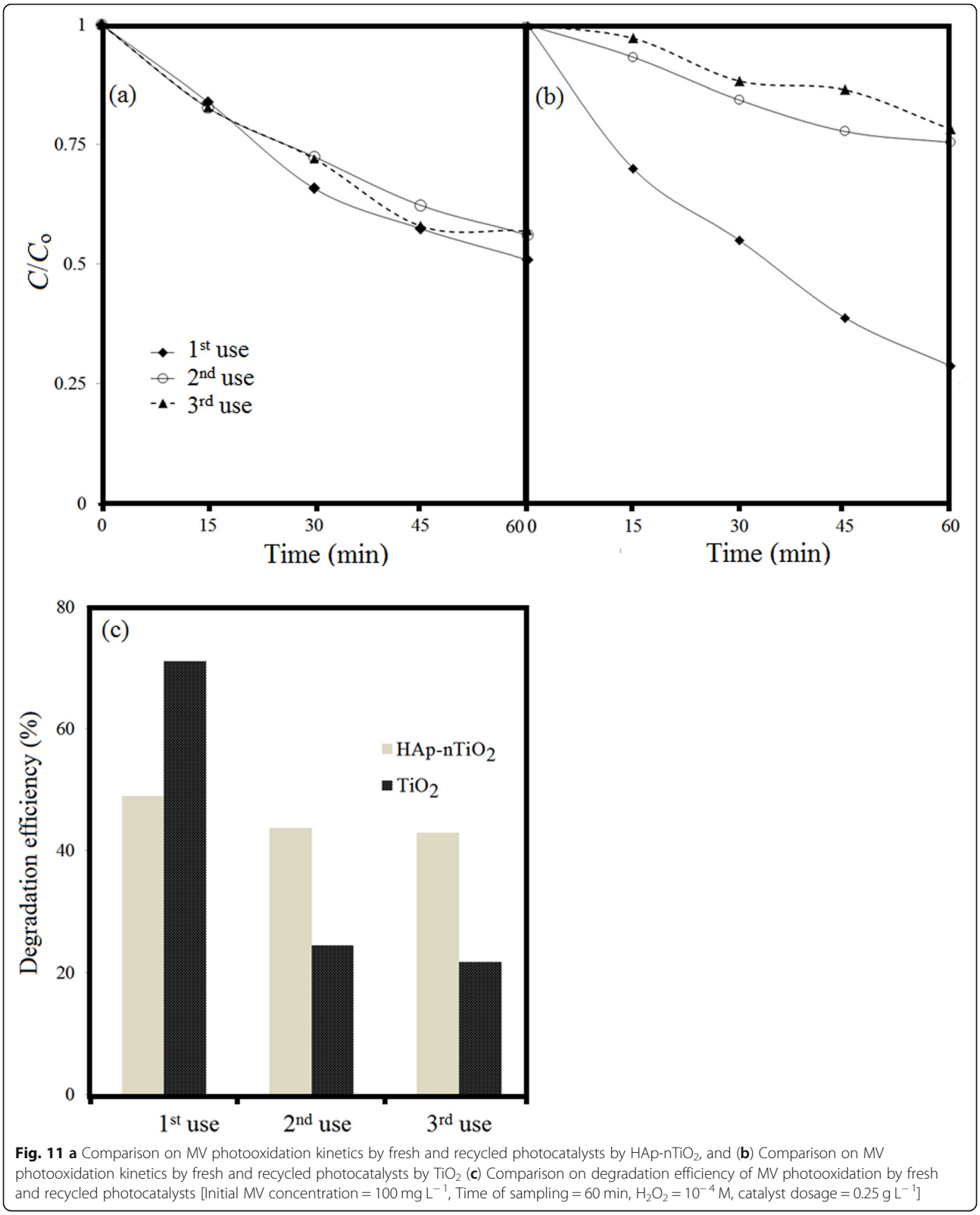

Fig. 11 **a** Comparison on MV photooxidation kinetics by fresh and recycled photocatalysts by HAp-nTiO_2, and (**b**) Comparison on MV photooxidation kinetics by fresh and recycled photocatalysts by TiO_2 (**c**) Comparison on degradation efficiency of MV photooxidation by fresh and recycled photocatalysts [Initial MV concentration = 100 mg L^{-1}, Time of sampling = 60 min, $H_2O_2 = 10^{-4}$ M, catalyst dosage = 0.25 g L^{-1}]

Acknowledgements
The authors wish to express sincere thanks to Directorate of Academic Development Universitas Islam Indonesia for financial support in proofreading service.

Authors' contributions
IF carried out the design of research, instrumental analysis interpretation of materials, and writing the manuscript. DF, TH, IS and CSR participated in material characterization experiments and kinetics data analysis especially simulation on photodegradation reaction experiment. AK participated in the design of the study, SEM-EDX analysis, and drafted the manuscript. All authors read and approved the final manuscript.

Funding
This research was funded by Advance Material for Energy and Environment (MEE) Laboratory, Chemistry Department of Universitas Islam Indonesia with laboratory facility by the grant (MEE/ChemDept/XII/2018).

Availability of data and materials
All data generated or analyzed during this study are available from the corresponding author on reasonable request.

Competing interests
The authors declare that they have no competing interests.

Author details
[1]Chemistry Department, Universitas Islam Indonesia, Yogyakarta 55584, Indonesia. [2]Chemistry Department, Universiti Pendidikan Sultan Idris Perak, 35900 Tanjong Malim, Perak, Malaysia.

Received: 23 January 2019 Accepted: 12 November 2019
Published online: 18 December 2019

References

1. Deng Y, Zhao RZ. Advanced oxidation processes (AOPs) in wastewater treatment. Curr Pollut Rep. 2015;1:167–76.
2. Hassaan MA, Nemr AE. Health and environmental impacts of dyes: mini review. Am J Environ Sci Eng. 2017;1:64–7.
3. Yanto DHY, Tachibana S, Itoh K. Biodecolorization and biodegradation of textile dyes by the newly isolated saline-pH tolerant fungus *Pestalotiopsis* sp. J Environ Sci Technol. 2014;7:44–55.
4. Mohammadi A, Aliakbarzadeh Karimi A, Fallah MH. Adsorption and photocatalytic properties of surface-modified TiO_2 nanoparticles for methyl orange removal from aqueous solutions. Prog Color Colorants Coat. 2016;9: 249–60.
5. Shang X, Li B, Zhang T, Li C, Wang X. Photocatalytic degradation of methyl orange with commercial organic pigment sensitized TiO_2. Procedia Environ Sci. 2013;18:478–85.
6. Pinho L, Mosquera MJ. Photocatalytic activity of TiO_2-SiO_2 nanocomposites applied to buildings: influence of particle size and loading. Appl Catal B-Environ. 2013;134:205–21.
7. Liu HF, Jia ZG, Ji SF, Zheng YY, Li M, Yang H. Synthesis of $TiO_2/SiO_2@Fe_3O_4$ magnetic microspheres and their properties of photocatalytic degradation dyestuff. Catal Today. 2011;175:293–8.
8. Liu C, Chen Z, Miao Z, Chen F, Gu C, Huang M, et al. Properties and preparation of porous carbon material supported with modified TiO_2. Procedia Eng. 2012;27:557–63.
9. Charlena, Suparto IH, Putri DK. Synthesis of hydroxyapatite from rice fields snail shell (*Bellamya javanica*) through wet method and pore modification using chitosan. Procedia Chem. 2015;17:27–35.
10. Fatimah I, Ilahi RN, Pratami R. Low cost $CaTiO_3$ perovskite synthesized from scallop (*Anadara granosa*) shell as antibacterial ceramic material. IOP Conf Ser-Mat Sci. 2018;299:012034.
11. Hadiyanto H, Lestari SP, Widayat W. Preparation and characterization of *Anadara Granosa* shells and $CaCO_3$ as heterogeneous catalyst for biodiesel production. Bull Chem React Eng. 2016;11:21–6.
12. Nurhayati M, Linggawati A, Anita S, Amri TA. Preparation and characterization of calcium oxide heterogeneous catalyst derived from *Anadara Granosa* shell for biodiesel synthesis. KnE Eng. 2016;2016:1–8.
13. Jamarun N, Azharman Z, Zilfa SU. Effect of firing for synthesis of hydroxyapatite by precipitation method. Orient J Chem. 2016;32:2095–9.
14. Kongsri S, Janpradit K, Buapa K, Techawongstien S, Chanthai S. Nanocrystalline hydroxyapatite from fish scale waste: preparation, characterization and application for selenium adsorption in aqueous solution. Chem Eng J. 2013;215:522–32.
15. Salma-Ancane K, Stipniece L, Locs J, Lakevics V, Irbe Z, Berzina-Cimdina L. The influence of biogenic and synthetic starting materials on the properties of porous hydroxyapatite bioceramics. Key Eng Mater. 2014;614:11–6.
16. Rujitanapanich S, Kumpapan P, Wanjanoi P. Synthesis of hydroxyapatite from oyster shell via precipitation. Enrgy Proced. 2014;56:112–7.
17. Anjaneyulu U, Pattanayak DK, Vijayalakshmi U. Snail shell derived natural hydroxyapatite: effects on NIH-3T3 cells for orthopedic applications. Mater Manuf Process. 2016;31:206–16.
18. Fatimah I, Aulia GR, Puspitasari W, Nurillahi R, Sopia L, Herianto R. Microwave-synthesized hydroxyapatite from paddy field snail (*Pila ampullacea*) shell for adsorption of bichromate ion. Sustain Environ Res. 2018;28:462–71.
19. Shariffuddin JH, Jones MI, Patterson DA. Greener photocatalysts: hydroxyapatite derived from waste mussel shells for the photocatalytic degradation of a model azo dye wastewater. Chem Eng Res Des. 2013;91: 1693–704.
20. Giannakopoulou T, Todorova N, Romanos G, Vaimakis T, Dillert R, Bahnemann D, et al. Composite hydroxyapatite/TiO_2 materials for photocatalytic oxidation of NO_x. Mater Sci Eng B-Adv. 2012;177:1046–52.
21. Oktar FN. Hydroxyapatite-TiO_2 composites. Mater Lett. 2006;60:2207–10.
22. Monmaturapoj N, Thepsuwan W, Mai-Ngam K, Ngernpimai S, Klinsukhon W, Prahsarn C. Preparation and properties of hydroxyapatite/titania composite for microbial filtration application. Adv Appl Ceram. 2014;113:267–74.
23. Sassoni E, D'Amen E, Roveri N, Scherer GW, Franzoni E. Photocatalytic hydroxyapatite-titania nanocomposites for preventive conservation of marble. IOP Conf Ser-Mat Sci. 2018;364:012073.
24. Buasri A, Chaiyut N, Loryuenyong V, Worawanitchaphong P, Trongyong S. Calcium oxide derived from waste shells of mussel, cockle, and scallop as the heterogeneous catalyst for biodiesel production. Sci World J. 2013;2013:460923.
25. Asimeng BO, Fianko JR, Kaufmann EE, Tiburu EK, Hayford CF, Anani PA, et al. Preparation and characterization of hydroxyapatite from *Achatina achatina* snail shells: effect of carbonate substitution and trace elements on defluoridation of water. J Asian Ceramic Soc. 2018;6:205–12.
26. Agbozu IE, Emoruwa FO. Batch adsorption of heavy metals (Cu, Pb, Fe, Cr and Cd) from aqueous solutions using coconut husk. Afr J Environ Sci Technol. 2014;8:239–46.
27. Tsuruoka A, Isobe T, Matsushita S, Wakamura M, Nakajima A. Comparison of photocatalytic activity and surface friction force variation on Ti-doped hydroxyapatite and anatase under UV illumination. J Photoch Photobio A. 2015;311:160–5.
28. Hu M, Yao ZH, Liu X, Ma LP, He Z, Wang XQ. Enhancement mechanism of hydroxyapatite for photocatalytic degradation of gaseous formaldehyde over TiO_2/hydroxyapatite. J Taiwan Inst Chem E. 2018;85:91–7.
29. Reddy MP, Venugopal A, Subrahmanyam M. Hydroxyapatite photocatalytic degradation of calmagite (an azo dye) in aqueous suspension. Appl Catal B-Environ. 2007;69:164–70.
30. Salhi A, Aarfane A, Tahiri S, Khamliche L, Bensitel M, Bentiss F, et al. Study of the photocatalytic degradation of methylene blue dye using titanium-doped hydroxyapatite. Mediterr J Chem. 2015;4:59–67.
31. Chen TW, Zheng YH, Lin JM, Chen GN. Study on the photocatalytic degradation of methyl orange in water using Ag/ZnO as catalyst by liquid chromatography electrospray ionization ion-trap mass spectrometry. J Am Soc Mass Spectrom. 2008;19:997–1003.
32. Serpone N, Salinaro A, Emeline A, Ryabchuk V. Turnovers and photocatalysis: a mathematical description. J Photoch Photobio A. 2000;130:83–94.
33. Yang SJ, Xu YL, Huang YK, Zhou GH, Yang ZY, Yang Y, et al. Photocatalytic degradation of methyl violet with $TiSiW_{12}O_{40}/TiO_2$. Int J Photoenergy. 2013; 2013:191340.
34. Liu W, Qian GM, Liu LL, Fan XY, Cai XY, Feng JY, et al. The growth mechanism of titania/hydroxyapatite and its application in the photodegradation of methyl orange dye under UV irradiation. Results Phys. 2018;11:112–7.
35. Ouinani EA, Boumanchar I, Zbair M, Chhiti Y, Sahibed-Dine A, Bentiss F, et al. The photocatalytic degradation of methylene bleu over TiO_2 catalysts supported on hydroxyapatite. J Mater Environ Sci. 2017;8:1301–11.
36. Teixeira S, Martins PM, Lanceros-méndez S, Kühn K, Cuniberti G. Reusability of photocatalytic TiO_2 and ZnO nanoparticles immobilized in

poly(vinylidene difluoride)-*co*-trifluoroethylene. Appl Surf Sci. 2016;384:497–504.
37. Deus F, Continentino MA. Superconductor-normal metal quantum phase transition in dissipative and non-equilibrium systems. Philos Mag. 2013;93:3062–80.
38. Khezrianjoo S, Revanasiddappa HD. Langmuir-Hinshelwood kinetic expression for the photocatalytic degradation of metanil yellow aqueous solutions by ZnO catalyst. Chem Sci J. 2012;2012:CSJ85.

Publisher's Note